

Analysis of Al 6061 and Mild Steel Joints from Rotary Friction Welding



Nikhil Gotawala and Amber Shrivastava

Abstract This work focuses on the microstructure evolution upon rotary friction welding of Al 6061 to mild steel and resulting joint strength. Material deforms plastically during rotary friction welding; however, temperatures are low enough to prevent melting, which limits intermetallic compound formation. Displacement-controlled rotary friction welding of circular workpieces is performed with combinations of three friction times (48, 24 and 16 s) and two rotation speeds (1200 and 1400 rpm). Significant grain refinement is observed at the centre on Al 6061 side, which indicates dynamic recrystallization. However, only recovery is observed at the mild steel side, which is attributed to low temperatures. The maximum joint strength of 136 MPa is achieved. The fractured surfaces from tensile tests reveal sticking of Al 6061 on mild steel at the centre region. The fractured surfaces suggest ductile fracture in the centre region and brittle fracture close to the periphery.

Keywords Rotary friction welding · Dissimilar material joining · Dynamic recrystallization

Introduction

Many industries like aerospace, automotive, marine, etc. desire to reduce the fuel consumption, for achieving lower operational cost and environmental impact. Lightweighting of structures without compromising strength is a potential way forward. Al alloys are light in weight with high specific strength. However, complete replacement of steel components by Al alloys is difficult due to higher price of Al alloys. This makes it desirable to join Al alloys and steel. Fusion welding of Al alloys and steels leads to large amount of brittle intermetallic compounds (IMC) in the joint, which deteriorate the joint's mechanical performance [1, 2]. The solid-state joining techniques, such as friction stir welding can be used for joining dissimilar

N. Gotawala · A. Shrivastava (✉)
Department of Mechanical Engineering, Indian Institute of Technology Bombay, Mumbai
400076, India
e-mail: ashrivastava.me@iitb.ac.in

materials [3]. Many researchers have successfully joined aluminium alloys and steel using friction stir welding [4, 5]. However, friction stir welding is limited to sheet- or plate-type components. Rotary friction welding (RFW) is a solid-state joining process, which can be used for joining circular components [6]. During RFW, one of the workpiece rotates about its axis and plunges into the stationary workpiece. The friction at the interface of the two workpieces leads to heat generation and the temperature rises, material deforms plastically and workpieces are forged together to create the joint. For dissimilar materials, the diffusion between two materials at the interface leads to the formation of IMC [7]. Further in the vicinity of the interface, dynamic recrystallization due to high temperature plastic deformation results in the grain refinement [8].

Over the last decade, many researchers have tried RFW with different combinations of materials. Liag et al. RFWed Al 1060 and Mg AZ 31 alloys at different friction pressures. Al_3Mg_2 and $\text{Al}_{12}\text{Mg}_{17}$ IMCs were observed at the interface and the joint tensile strength improved with increase in friction pressure up to a certain value [9]. Guo et al. also found Al_3Mg_2 and $\text{Al}_{12}\text{Mg}_{17}$ IMCs in RFWed joints of 7A04 Al alloy and Mg AZ 31 alloy [10]. The IMC thickness decreased significantly with increase in friction pressure. Ma et al. successfully joined 1045 carbon steel and 304 stainless steel with RFW, and analysed formation of carbide layer (CrC and Cr_{23}C_6) at the interface due to diffusion [11]. Similarly, Celik et al. performed RFW of AISI 4140 and AISI 1050 steels. The joint tensile strength was comparable to the parent materials and hardness improved near interface due to grain refinement [12]. Satyanarayana et al. optimized the tensile strength of RFWed austenitic and ferritic steel with respect to process parameters [13]. Li et al. studied effect of tool rotation speed on RFW Ti alloy and stainless steel joints [14]. The joint strength increased with increase in tool rotational speed up to a critical value and decreased thereafter. FeTi and Fe_2Ti IMCs were reported at the interface of Ti alloy and stainless steel [14]. Dev et al. also observed comparable joint strength of RFWed Ti and SS 304 joints as compared against the Ti. However ductility was extremely poor upon bend test due to presence of IMCs at the interface. Post-weld heat treatment led to improvement in the ductility of the RFWed joints [15].

Some researchers have also attempted to weld aluminium alloys with steels using RFW. Sundaresan et al. performed RFW of aluminium alloy and austenitic stainless steel [16]. Fe_2Al_5 and FeAl_3 IMCs were reported at the joint interface [16]. Taban et al. reported Fe_2Al_5 and FeAl IMCs in RFWed joints of Al 6061 and AISI 1081 steel [17]. Fukumoto et al. noticed Fe_2Al_5 , FeAl_3 and FeAl IMCs at the interface of Al 1050 and austenitic stainless steel joints from RFW [18]. The elongation of aluminium grains was observed in the vicinity of weld interface due to deformation during process. The flying surface of stainless steel also underwent austenite to martensite phase transformation [18]. Fukumoto et al. observed that the joint tensile strength is maximum for a certain friction time and decreases on either increasing or decreasing the friction time, for RFWed Al 5052 and SS 304 joints [19]. Fukumoto et al. also found an amorphous layer at the interface of Al 5052 and SS 304 RFWed joints [20]. For majority of the existing work, RFW is performed in the pressure control mode. In the present work, RFW of Al 6061 and mild steel is attempted

with displacement control. The RFWed joints of Al 6061 and mild steel are prepared with different rotation speeds and friction times. The RFWed joints are subjected to tensile test and microstructure at the joint interface is analysed. The fracture surfaces of tensile specimens are also studied to determine the fracture mechanism of the weld.

Experimental Work

RFW of Al 6061 and mild steel were performed on three-axis CNC mill (LMW LV55). The length and diameter of the mild steel and Al 6061 rods are 100 mm and 12 mm, respectively. Figure 1 shows the schematic diagram of RFW of Al 6061 and mild steel. During RFW, mild steel rod was rotating and Al 6061 rod was held stationary. A dwell time of 5 s was provided to remove initial oxide layer and improve the heat generation. Next, the rotating mild steel rod was plunged to a depth of 8 mm into the Al 6061 rod (Friction action). The RFWed joints were created with three feed rates during 'Friction action': 10 mm/min, 20 mm/min, and 30 mm/min, which corresponded to friction times of 48 s, 24 s, and 16 s, respectively (for plunge to a depth of 8 mm). After 'Friction action', mild steel rod stopped rotating motion and plunged further by 10 mm into the Al 6061 rod at a feed rate of 100 mm/min (Forging action). Finally, the joint is allowed to cool. The Al 6061-mild steel RFW joints were performed at two rotation speeds: 1200 and 1400 rpm.

To determine the joint strength, tensile test was performed as per ASTM E8/E8M standard on Instron tensile testing machine. The gauge length and diameter of the tensile test specimen were 45 mm and 6 mm, respectively. Welding specimen cross section cut using wire EDM to see microstructure at interface of both material. The joints were cross-sectioned and polished. These samples were electro-polished used as a final polishing. Electro polishing performed on Buehler Electromet 4 with electrolyte (700 ml ethanol + 200 ml perchloric acid + 100 ml butanol) at 15 V and

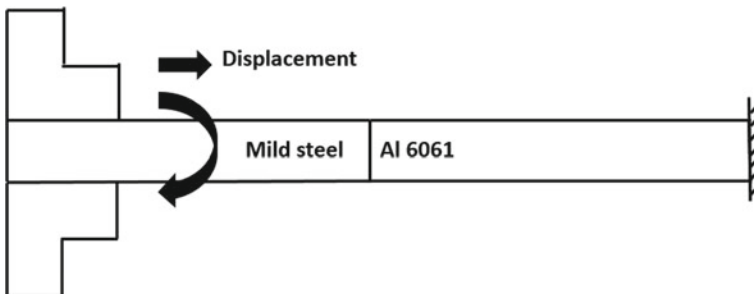


Fig. 1 Schematic of rotary friction welding of Al 6061 and mild steel

–10 °C for 20 s. Electron back scattered diffraction (EBSD) was done to analyse the microstructure at the joint interface. Gemini SEM 300 with EBSD detector was used for EBSD scans. EBSD scan was performed over $250\ \mu\text{m} \times 250\ \mu\text{m}$ with step size of $0.5\ \mu\text{m}$. Aztec HKL was used to analyse the EBSD scans.

Results and Discussion

Microstructure Evolution at Al 6061 and Mild Steel Interface

Figures 2 and 3 show the EBSD results at the interface of Al 6061 and mild steel RFWed joint prepared with rotation speed of 1200 rpm and friction time of (a) 48 s (b) 24 s (c) 16 s. For this analysis, a misorientation angle greater than 10° is considered as for identifying grains. Al 6061 and mild steel sides are shown in red and blue colours, respectively. A variation in grain size from interface towards Al 6061 side can be noticed. This is attributed to the dynamic recrystallization due to high temperature plastic deformation et al. 6061 side during RFW. In a similar observation, Winiczenko et al. also noticed dynamic recrystallization of Al 5454 alloy upon RFW with a tungsten heavy alloy [21]. From Figs. 2 and 3, finer grains can be noticed near the interface at the Al 6061 side. From the samples welded at 1200 rpm rotation speed and friction time of 48 s, 24 s, and 16 s, the average size of Al 6061 alloy grains are $3.3\ \mu\text{m}$, $3.4\ \mu\text{m}$, and $5.2\ \mu\text{m}$, respectively. Similarly, from the samples welded at 1400 rpm rotation speed and friction time of 48 s, 24 s, and 16 s, the average size of Al 6061 alloy grains are $6.1\ \mu\text{m}$, $5.3\ \mu\text{m}$, and $4.4\ \mu\text{m}$, respectively.

During RFW, higher rotation speed and friction times lead to higher temperatures [9, 14], which encourage grain growth after recrystallization. Also, higher rotation speed and friction times lead to more accumulation of strain, which promotes grain refinement [22]. The interplay of these effects is well reflected by the average grain size of Al 6061 (near joint interface) across the RFWed Al 6061-mild steel joints. At higher rotation speed of 1400 rpm, the average Al 6061 grain size increases with increase in friction time, and this suggests that the grain growth owing to higher temperatures is significant. At the lower rotation speed of 1200 rpm, the grain size reduces as the friction time increases from 16 to 24 s. This suggests that the accumulation for strain at higher friction time of 24 s is more pronounced than the additional grain growth that would be achieved due to increased temperature (compared to friction time of 16 s at 1200 rpm). However further increase in friction time to 48 s from 24 s at 1200 rpm affects the average Al 6061 grain size minimally. This suggests that the increased accumulation of strain at higher friction time of 48 s is countered by the additional grain growth owing to higher temperature (compared to friction time of 24 s at 1200 rpm).

At the steel side of the joint interface, a non-indexed region is observed in EBSD scans of all the RFWed joint samples. This is expected to be a high dislocation density

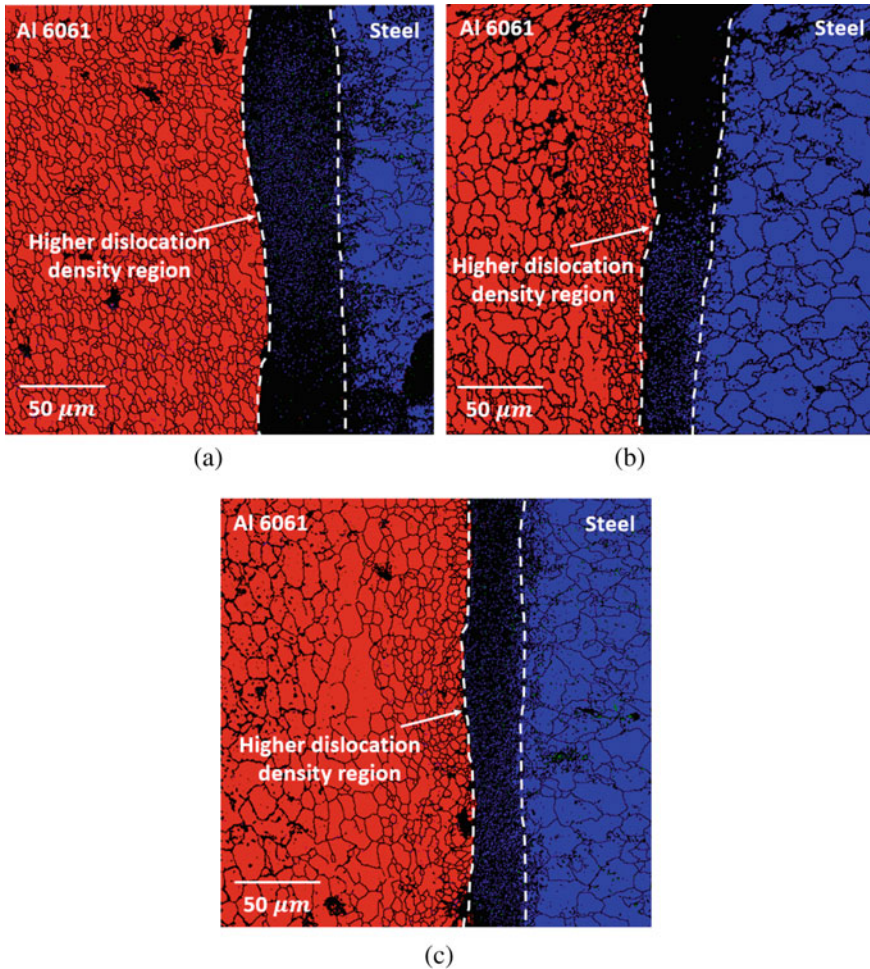


Fig. 2 EBSD et al. 6061 and mild steel interface of RFWed joint performed at 1200 rpm and friction time of **a** 48 s **b** 24 s and **c** 16 s. (Color figure online)

region on the steel side of the joint interface. The non-indexed region suggests that there was no dynamic recrystallization on the steel side. This is suspected due to process temperatures lower than the dynamic recrystallization temperature for steel. For the joints RFWed at 1200 rpm rotation speed and friction times of 48 s, 24 s, and 16 s, the average width of the non-indexed regions are 53.8 μm , 34.6 μm , and 28.9 μm , respectively. Similarly, for the joints RFWed at 1400 rpm rotation speed and friction times of 48 s, 24 s, and 16 s, the average width of the non-indexed regions are 18.3 μm , 9.9 μm , and 5.6 μm , respectively. The width of the non-indexed region reduced with increase in rotation speed. This is anticipated due to more recovery at

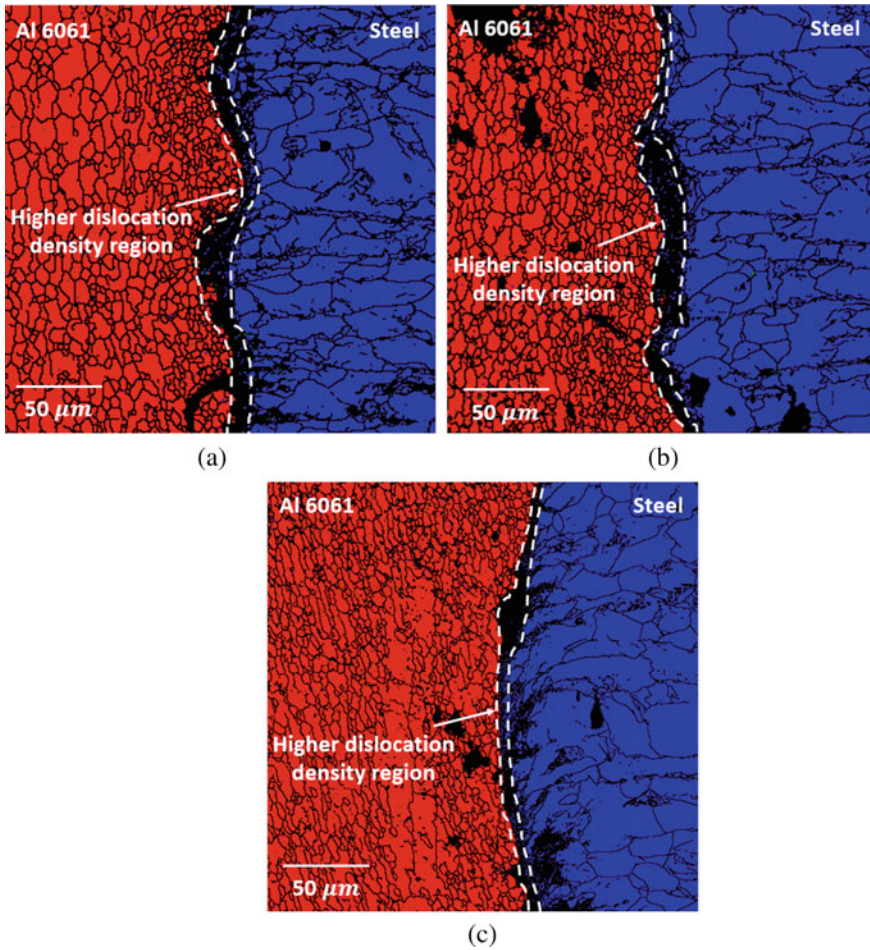


Fig. 3 EBSD et al. 6061 and mild steel interface of RFWed joint performed at 1400 rpm and friction time of **a** 48 s **b** 24 s and **c** 16 s. (Color figure online)

higher temperature with increase in rotation speed. There is also reduction in non-indexed region with decrease in friction time. This is due to reduction in accumulation of strain with decrease in friction time.

Tensile Strength and Fracture Surface Analysis

Figure 4 shows tensile strength of RFWed joints prepared with different rotation speeds and friction times. The maximum tensile strength of observed all the joint samples is 136 MPa. As figure shows the tensile strength of weld is higher for the

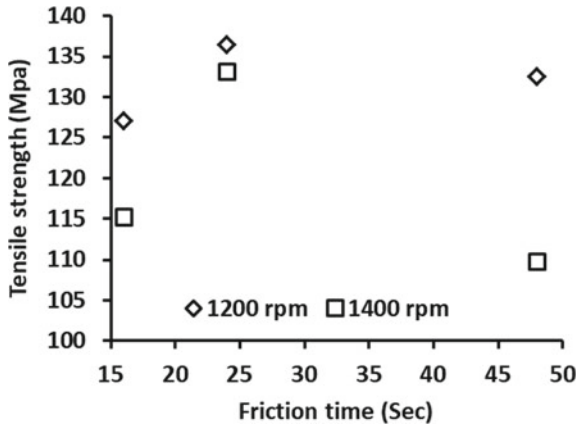


Fig. 4 Tensile strength of RFWed joints prepared with different rotation speeds and friction times

samples joined at 1200 rpm as compared to the samples joined at 1400 rpm, for all the friction times. This may be due to smaller amount of brittle IMC formation at lower temperatures, owing to lower rotation speed. With respect to friction time, the maximum tensile strength is recorded for the samples joined with 24 s, for both the rotation speeds. This suggests that diffusion at Al6061-steel interface is not sufficient at lower friction time (16 s), while excessive diffusion at higher friction (48 s) would have led to more brittle IMCs.

Fracture surfaces from tensile tests are analysed to study the nature of failure. Figure 5a–c shows the fractured Al6061 surfaces from the joints prepared at 1200 rpm with friction time of 48 s, 24 s, and 16 s, respectively. Similarly, Fig. 6(a–c) shows the fractured Al6061 surfaces from the joints prepared at 1400 rpm with friction time of 48 s, 24 s, and 16 s, respectively. Circular marks can be noticed at the fractured surfaces of all the samples. Circular marks appear to follow the material flow during the process and rough surface indicates towards possible brittle failure. From Figs. 5b

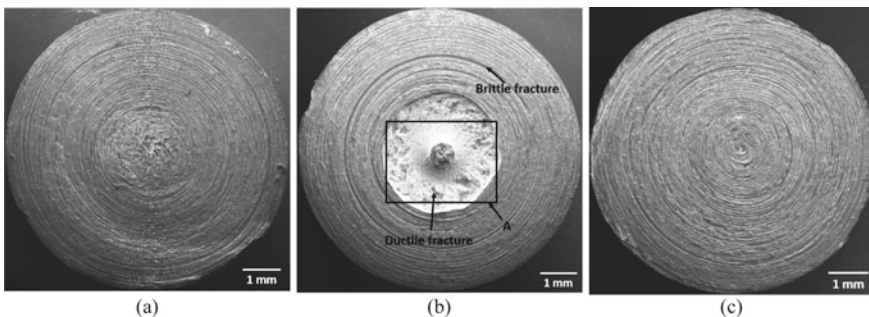


Fig. 5 Fractured Al6061 surface from the joint prepared at 1200 rpm with friction time of **a** 48 s **b** 24 s and **c** 16 s

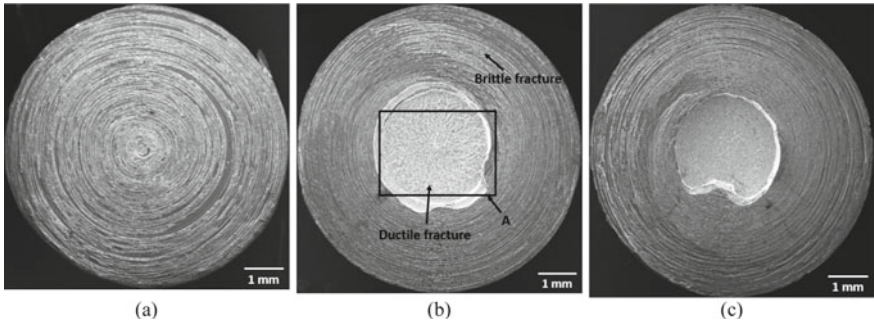


Fig. 6 Fractured Al6061 surface from the joint prepared at 1400 with friction time of **a** 48 s **b** 24 s and **c** 16 s

and **6b**, it can be noticed that the chunk of aluminium alloy broke away from the centre region (location A). Figures **7** and **8** shows the locations A of Fig. **5a** and **6a** at higher magnification. The presence of dimple features at locations A suggests

Fig. 7 Fractured Al6061 surface at location A of the joint prepared with 1200 and 24 s friction time

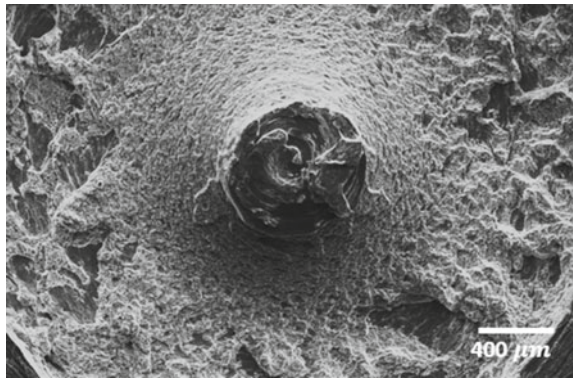
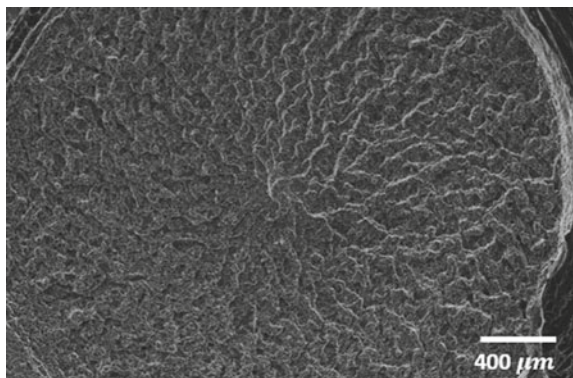


Fig. 8 Fractured Al6061 surface at location A of the joint prepared with 1400 and 24 s friction time



the ductile nature of failure at the centre and nearby regions of the samples joined with 24 s friction time. This implies that the ductile fracture occurred at the centre and brittle fracture occurred at the peripheral locations, for the sample with the maximum tensile strength in this study. This observation is consistent with variation in IMC thickness observed by Fukumoto et al. along the radius for RFWed samples [20]: minimum IMCs at the centre and along the radial direction increase towards periphery. This can be attributed to lower heat generation in the centre region due to slower relative motion between two materials.

Conclusions

The present work is focused on RFW of Al 6061 and steel with the displacement control mode. The RFW was performed with the combinations of two rotation speeds (1200 and 1400 rpm) and three friction times (48, 24 and 16 s). Microstructural analysis by EBSD at the Al6061-steel interface of the joints suggests dynamic recrystallization et al. 6061 side and grain size of Al 6061 in the vicinity of the interface depends on the RFW process parameters. However, recrystallization is not observed at the steel side of the Al6061-steel interface. Instead, a non-indexed region is noticed at the steel side next to the joint interface. This is expected due to accumulation of strains upon plastic deformation during RFW. The size of non-indexed region reduced with increase in rotation speed, due to improved recovery at higher temperatures at higher rotation speed. The maximum tensile strength of 136 MPa is recorded for the joint prepared at 1200 rpm rotation speed and 24 s friction time. The inspection of fracture surface revealed that ductile fracture occurred at the centre and brittle fracture occurred at the peripheral locations, for the sample with the maximum tensile strength in this study. This observation is consistent with the variation in IMC thickness along the radius for RFWed samples observed in previous study.

Acknowledgements The authors gratefully acknowledge the partial support of this work by the Science & Engineering Research Board, Department of Science & Technology, Government of India (File No. ECR/2017/000727/ES), Department of Mechanical Engineering, Microstructural Mechanics and Microforming Lab and Machine Tools Lab at Indian Institute of Technology.

References

1. Mukherjee S, Chakraborty S, Galun R, Estrin Y, Manna I (2010) Transport phenomena in conduction mode laser beam welding of Fe–Al dissimilar couple with Ta diffusion barrier. *Int J Heat Mass Transf* 53(23–24):5274–5282
2. Sierra G, Peyre P, Deschaux-Beaume F, Stuart D, Fras G (2007) Steel to aluminium key-hole laser welding. *Mater Sci Eng, A* 447(1–2):197–208
3. Murr LE (2010) A review of FSW research on dissimilar metal and alloy systems. *J Mater Eng Perform* 19(8):1071–1089

4. Movahedi M, Kokabi AH, Reihani SS, Najafi H (2012) Effect of tool travel and rotation speeds on weld zone defects and joint strength of aluminium steel lap joints made by friction stir welding. *Sci Technol Weld Joining* 17(2):162–167
5. Chen TP, Lin WB (2010) Optimal FSW process parameters for interface and welded zone toughness of dissimilar aluminium–steel joint. *Sci Technol Weld Joining* 15(4):279–285
6. Li W, Vairis A, Preuss M, Ma T (2016) Linear and rotary friction welding review. *Int Mater Rev* 61(2):71–100
7. Lee WB, Bang KS, Jung SB (2005) Effects of intermetallic compound on the electrical and mechanical properties of friction welded Cu/Al bimetallic joints during annealing. *J Alloy Compd* 390(1–2):212–219
8. Liu FC, Nelson TW (2018) Grain structure evolution, grain boundary sliding and material flow resistance in friction welding of Alloy 718. *Mater Sci Eng, A* 710:280–288
9. Liang Z, Qin G, Wang L, Meng X, Li F (2015) Microstructural characterization and mechanical properties of dissimilar friction welding of 1060 aluminum to AZ31B magnesium alloy. *Mater Sci Eng, A* 645:170–180
10. Guo W, You G, Yuan G, Zhang X (2017) Microstructure and mechanical properties of dissimilar inertia friction welding of 7A04 aluminum alloy to AZ31 magnesium alloy. *J Alloy Compd* 695:3267–3277
11. Ma H, Qin G, Geng P, Li F, Fu B, Meng X (2015) Microstructure characterization and properties of carbon steel to stainless steel dissimilar metal joint made by friction welding. *Mater Des* 86:587–597
12. Celik S, Ersozlu I (2009) Investigation of the mechanical properties and microstructure of friction welded joints between AISI 4140 and AISI 1050 steels. *Mater Des* 30(4):970–976
13. Satyanarayana VV, Reddy GM, Mohandas T (2005) Dissimilar metal friction welding of austenitic–ferritic stainless steels. *J Mater Process Technol* 160(2):128–137
14. Li X, Li J, Liao Z, Jin F, Zhang F, Xiong J (2016) Microstructure evolution and mechanical properties of rotary friction welded TC4/SUS321 joints at various rotation speeds. *Mater Des* 99:26–36
15. Dey HC, Ashfaq M, Bhaduri AK, Rao KP (2009) Joining of titanium to 304L stainless steel by friction welding. *J Mater Process Technol* 209(18–19):5862–5870
16. Sundaresan S, Murti KGK (1993) Friction welding of aluminium to austenitic stainless steel. *Int J Joining Mater* 5:66–66
17. Taban E, Gould JE, Lippold JC (2010) Dissimilar friction welding of 6061-T6 aluminum and AISI 1018 steel: properties and microstructural characterization. *Mater Des* (1980–2015), 31(5):2305–2311
18. Fukumoto S, Tsubakino H, Okita K, Aritoshi M, Tomita T (1998) Microstructure of friction weld interface of 1050 aluminium to austenitic stainless steel. *Mater Sci Technol* 14(4):333–338
19. Fukumoto S, Tsubakino H, Okita K, Aritoshi M, Tomita T (1999) Friction welding process of 5052 aluminium alloy to 304 stainless steel. *Mater Sci Technol* 15(9):1080–1086
20. Fukumoto S, Tsubakino H, Okita K, Aritoshi M, Tomita T (2000) Amorphization by friction welding between 5052 aluminum alloy and 304 stainless steel. *Scripta Materialia* 42(8)
21. Winiczenko R, Goroch O, Krzyńska A, Kaczorowski M (2017) Friction welding of tungsten heavy alloy with aluminium alloy. *J Mater Process Technol* 246:42–55
22. Midling OT, Grong Ø (1994) A process model for friction welding of Al–Mg–Si alloys and Al–SiC metal matrix composites—I. Haz temperature and strain rate distribution. *Acta Metallurgica et Materialia* 42(5):1595–1609